

COURSE 10

**INVERSE METHODS  
IN OCEAN BOTTOM ACOUSTICS**

G.V. FRISK

*Woods Hole Oceanographic Institution  
Woods Hole, Massachusetts 02543, USA*

*Y. Desaubies, A. Tarantola and J. Zinn-Justin, eds.  
Les Houches, Session L, 1988  
Tomographie Océanographique et Géophysique /  
Oceanographic and Geophysical Tomography  
© Elsevier Science Publishers B.V., 1990*

## Contents

1. Introduction	413
2. Specific feature methods	414
2.1. Caustic range method	414
2.2. Advantages	417
2.3. Disadvantages	417
3. Iteration of forward models methods	417
3.1. Fitting near-bottom transmission loss	418
3.2. Advantages	421
3.3. Disadvantages	421
4. Perturbative inversion methods	422
4.1. Reflection coefficient inversion	423
4.2. Normal mode eigenvalue inversion	425
4.3. Advantages	428
4.4. Disadvantages	428
5. Exact inverse methods	429
5.1. Gelfand–Levitan method	430
5.2. Advantages	433
5.3. Disadvantages	434
6. Conclusions	434
References	435

## 1. Introduction

The determination of geoacoustic models for the bottom is of considerable importance in ocean acoustics. Knowledge of the acoustic properties of the bottom is generally required for accurate propagation modeling in the water column and plays a major role in inferring geological structure. We present a review of inverse methods used to determine the bottom parameters in both deep and shallow water. Existing techniques fall into one or more of the following four categories:

- (1) specific feature,
- (2) iteration of forward models,
- (3) perturbative inversion, and
- (4) exact inverse methods.

Rather than presenting an extensive literature survey, we focus on the basic concept underlying each one of the classes and provide examples of each type of approach from our own experience using synthetic and experimental data.

In general, we are interested in input data obtained in the water column using a narrowband or broadband point source and a point receiver or array of receivers. Our goal is to determine the density, the compressional wave speed and attenuation, and the shear wave speed and attenuation of the bottom as a function of position. In order to clarify the nature of the various methods, we examine the extremely important simplified case of the one dimensional, horizontally stratified, fluid bottom probed with a monochromatic source (cf. fig. 1).

We contend that techniques which address the more general problem may complicate the nature of the input data and the details of the inversion procedure, but nevertheless fall into one or more of the four categories described above. Furthermore, motivated by ocean acoustic applications, we concentrate on the frequency range 25–500 Hz, and the inference of the acoustic properties in the top few hundred meters of sediment with high resolution (<few meters in depth) and high accuracy (<10% error). Finally, the advantages and disadvantages of each class of techniques and implications for problems of higher dimensionality are discussed.

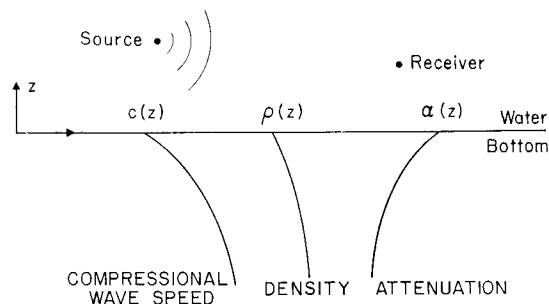


Fig. 1. One dimensional, horizontally stratified fluid bottom model.

## 2. Specific feature methods

In this case, specific dominant features of the data are related to certain geoaoustic parameters, and the resultant equations are “inverted” to obtain the desired parameters as a function of the features in the data. Conventional seismic travel time analysis [1] is an example of this approach. Here the arrival times of readily identifiable subbottom reflected and/or refracted paths are used to obtain velocity–depth functions. We examine in more detail the caustic range method described in ref. [2].

### 2.1. Caustic range method

Positive sound speed gradients in ocean bottom sediments can cause the formation of caustics in the acoustic field due to a point source located in the water. The caustics can extend into the water column and manifest themselves as high intensity regions in the field measured near the bottom. The horizontal range to the caustic depends upon the source/receiver heights above the bottom and the parameters of both the water and bottom sound speed profiles. For certain types of profiles, the analytic relationship among these quantities can be determined using the WKB approximation. We describe a method for determining the bottom sound speed profile which involves measuring ranges to the caustic at different source/receiver heights and using the WKB equations to calculate the parameters of the profile.

A characteristic water–bottom sound speed profile and the corresponding ray diagram illustrating caustic formation are shown in fig. 2. The principal features of the profile are: a weak positive gradient ( $\sim 0.016 \text{ s}^{-1}$ ) in the water; a drop in sound speed ( $\sim 1\text{--}2\%$  relative to the water sound speed) at the water–bottom interface; a strong positive gradient ( $\sim 1\text{--}2 \text{ s}^{-1}$ ) in the top sediment layer; and a strong subbottom reflector. The ray paths shown

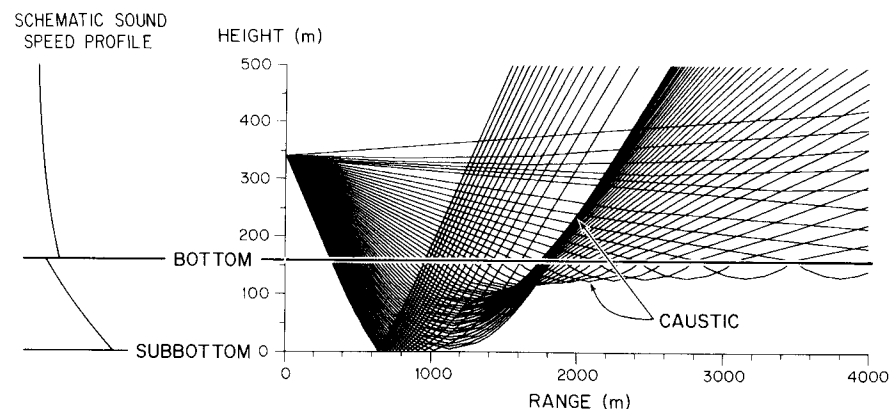


Fig. 2. Characteristic water–bottom sound speed profile and ray diagram.

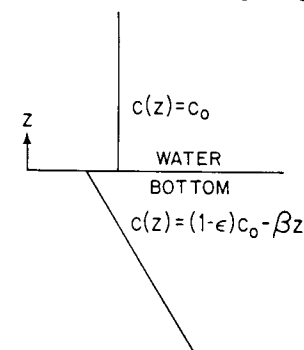


Fig. 3. Two-parameter bottom profile.

are those which dominate the bottom interaction at low frequencies and small grazing angles. These are the direct path, the subbottom reflected path, and the refracted path.

The refracted paths give rise to a caustic with two branches, one of which extends into the water column. Using the WKB approximation, we have calculated the caustic range  $r_c$  for the two-parameter bottom profile shown in fig. 3.

The result for  $r_c$  is:

$$r_c = \frac{2}{\beta} [2\beta c_0(z + z_0) + 4\epsilon c_0^2]^{1/2} \quad (1)$$

The calculation leading to eq. (1) involves, in addition to the WKB approximation, the following approximation:

$$\epsilon \ll \frac{\sin \theta_c}{\cos^2 \theta_c} \quad (2)$$

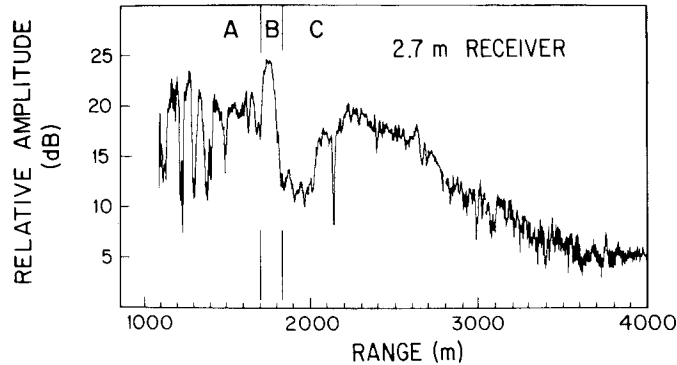


Fig. 4. Measured amplitude versus range at 220 Hz for 180 m source height and 2.7 m receiver height.

where  $\theta_c$  is the minimum grazing angle in the water associated with caustic formation. Usually  $\epsilon \ll 1$ , so that for typical gradients and the associated  $\theta_c$  this condition is satisfied. If we have one measurement of  $r_c$  and know either  $\beta$  or  $\epsilon$ , we can solve for the second parameter using either

$$\beta = \frac{4c_0}{r_c^2} \left\{ z + z_0 + [(z + z_0)^2 + \epsilon r_c^2]^{1/2} \right\} \quad (3a)$$

or

$$\epsilon = \frac{\beta^2 r_c^2}{16c_0^2} - \frac{\beta(z + z_0)}{2c_0} \quad (3b)$$

If we have two caustic range measurements  $r_{c1}$  and  $r_{c2}$  at receiver heights  $z_1$  and  $z_2$ , respectively, we can then solve for both  $\beta$  and  $\epsilon$  using

$$\beta = \frac{8c_0(z_1 - z_2)}{r_{c1}^2 - r_{c2}^2} \quad (4a)$$

and

$$\epsilon = \frac{1}{16c_0^2} [\beta^2 r_{c1}^2 - 8\beta c_0(z_1 + z_0)] \quad (4b)$$

We illustrate the method using 220 Hz data obtained in the Hatteras Abyssal Plain at 34°N, 67°W in 5150 m of water. The details of the experiment are described in ref. [3]. The observed amplitude versus range for a source height of 180 m and receiver height of 2.7 m is shown in fig. 4.

The amplitude exhibits a strong spatial interference pattern which arises from the combination of the direct and bottom-interacting steady-state signals. A peak is evident in region B of the data. This peak, in addition to having the maximum amplitude, has a shape which is clearly distinguishable as that due to the caustic with a corresponding range of 1750 m. Furthermore, we assume that  $\epsilon$  is known to be 0.016 from other work [3]. Using eq. (3a), we then obtain a value of  $0.94 \text{ s}^{-1}$  for  $\beta$ . This result is in close agreement with results obtained from a considerably more detailed analysis of the data [3].

## 2.2. Advantages

- Specific feature methods exploit a dominant physical effect into which a significant amount of acoustic energy is concentrated.
- Once the specific features are identified, the methods are relatively straightforward to implement.
- They tend to be stable with respect to the introduction of noise.

## 2.3. Disadvantages

- They typically do not use the entire available data set.
- When a specific feature becomes clouded by other effects, the method must be patched up, sometimes in an awkward way. An example is the complication associated with taking into account the subbottom reflector in the caustic range method.
- They provide no statement about uniqueness.
- They have effective, but limited, application to experimental data.
- They cannot always be generalized to problems of higher dimensionality since the specific feature may simply not exist in higher dimensions.

## 3. Iteration of forward models methods

This class of techniques is also called analysis by synthesis, parametric inversion, and trial and error inversion. In this approach, acoustic fields are computed theoretically for various values of the bottom parameters until the parameter set is found which provides a best fit to the data. The comparisons between theory and experiment are made visually or can be automated on the computer by searching for the parameter set which minimizes some measure of the difference between theory and experiment. The search through parameter space may be randomly prescribed or may

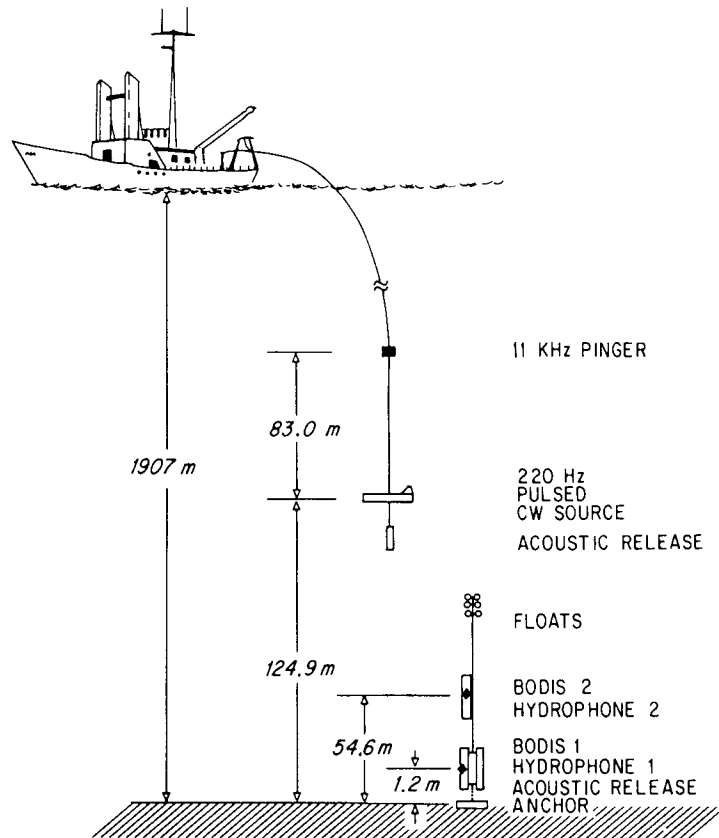


Fig. 5. Experimental configuration for the Icelandic Basin experiment.

be directed by linearizing the problem [4]. Fitting measured seismograms with theoretically generated ones is an example of this approach [1]. We will discuss in detail the example of fitting near-bottom measurements of transmission loss.

### 3.1. Fitting near-bottom transmission loss

Several experiments have been conducted [3,5] in which the amplitude and phase of the acoustic field at 220 Hz have been measured on a dense spatial grid (about every half-wavelength in range) in a near-bottom geometry. The experimental configuration and amplitude data for a site in the Icelandic Basin are shown in Figs.5 and 6, respectively.

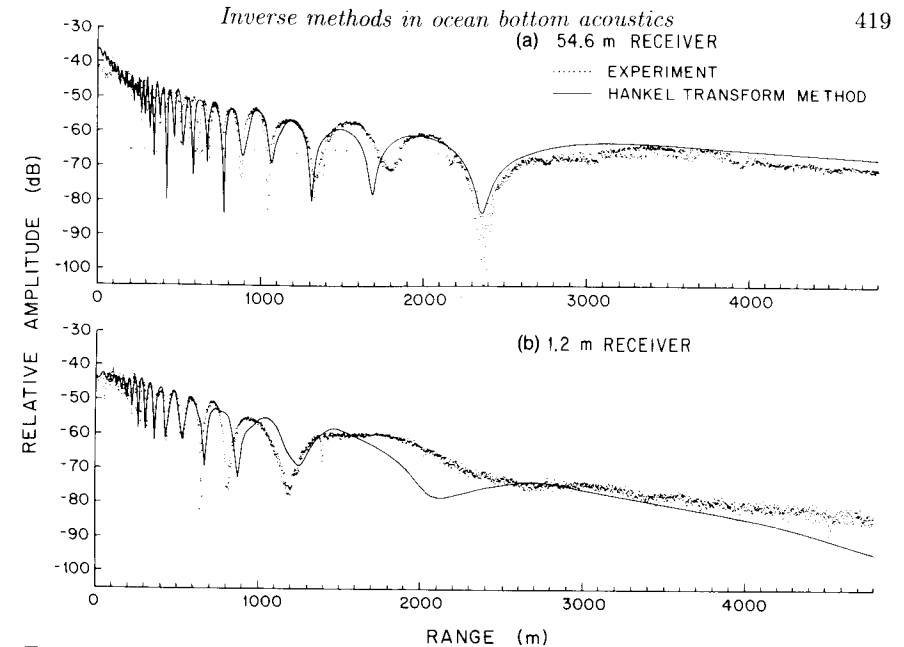


Fig. 6. Comparison of experimental data with Hankel transform results for the geoacoustic model in fig. 7.

The experiments were conducted in a pulsed *cw* mode, thus enabling the surface-reflected and water multiple arrivals to be gated out. The strong spatial interference patterns are therefore due to the coherent combination of the direct and bottom-interacting arrivals, which are dominated by paths of the type shown in fig. 2.

These data were analyzed by using the parabolic equation method (PEM) and a Hankel transform method (HTM) sequentially to compute acoustic fields for different bottom parameters until best fits to the data were obtained [5]. Typically, hundreds of runs of the PEM were executed in order to arrive at initial estimates of the values of sediment layer thickness, linear sound-speed gradient, and sound-speed discontinuity at the water-bottom interface. In automating this procedure, we estimated the layer thickness based on 3.5 kHz normal incidence records and varied the sound-speed gradient and discontinuity at the water-bottom interface until the mean square difference between the theoretical and experimental amplitudes in dB at both receivers was minimized. This operation was first performed on a coarse grid of reasonable values for the latter two parameters and then on a fine grid about the best coarse grid result. Specifically, the mean-square

difference  $\sigma^2$  is given by

$$\sigma^2 = \frac{1}{N} \sum_{n=1}^N [(x_{m_n} - \bar{x}_m) - (x_{t_n} - \bar{x}_t)]^2 \quad (5)$$

where  $N$  is the total number of measured data points,  $x_{m_n}(x_{t_n})$  is the  $n$ th experimental (theoretical) amplitude data point, and  $\bar{x}_m(\bar{x}_t)$  are the average experimental (theoretical) amplitude values:

$$\bar{x}_m = \frac{1}{N} \sum_{n=1}^N x_{m_n}, \quad (6a)$$

$$\bar{x}_t = \frac{1}{N} \sum_{n=1}^N x_{t_n}. \quad (6b)$$

Since the PEM is based on an approximation to the wave equation and does not accommodate a comprehensive geoacoustic model, we used the HTM to refine the parameters obtained from the PEM and to determine values for the remaining parameters in the geoacoustic model. In principle, the HTM provides an exact solution to the wave equation in horizontally stratified environments. It is based on the numerical evaluation of the Hankel transform for the pressure as a function of range [ $\exp(-i\omega t)$  time dependence is suppressed throughout ]

$$p(r) = \int_0^\infty g(k_r) J_0(k_r r) k_r dk_r, \quad (7)$$

where

$$g(k_r) = \frac{i}{k_z} \left[ e^{ik_z |z - z_0|} + R(k_r) e^{ik_z (z + z_0)} \right] \quad (8)$$

is the depth-dependent Green's function and  $R(k_r)$  is the plane-wave reflection coefficient of the bottom. Here  $k_r$  is the horizontal wavenumber,  $k_z = \sqrt{k_0^2 - k_r^2}$  is the vertical wavenumber in the water,  $k_0 = \omega/c_0$  is the water wavenumber,  $J_0(\cdot)$  is the Bessel function of order zero, and  $z_0$  and  $z$  are the source and receiver heights, respectively. Typically, tens of runs of the HTM were executed, and visual comparisons were then made between theory and experiment. The geoacoustic model inferred from this procedure is shown in fig. 7.

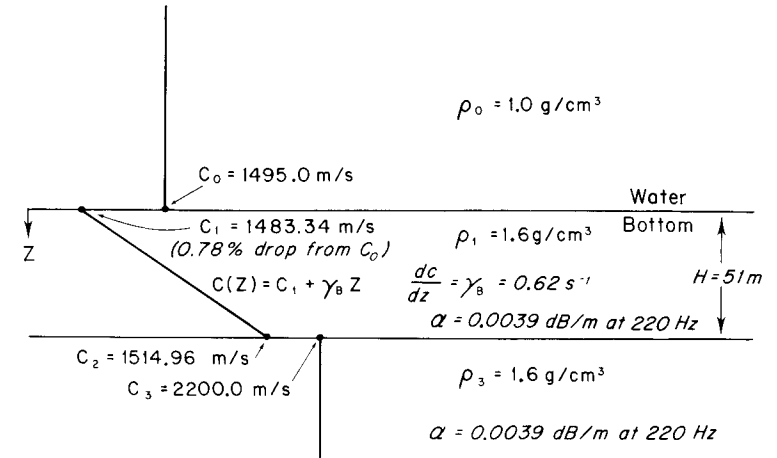


Fig. 7. Geoacoustic model inferred from the data using iteration of forward models.

The corresponding excellent comparisons between theory and experiment are shown in fig. 6. The associated minimum in the mean square difference [cf. eq. (5)] for the inferred sound-speed gradient, with fixed layer thickness and sound-speed drop, is shown in fig. 8.

### 3.2. Advantages

- Iteration of forward models methods utilize most or all of the data available.
- They appear to be the most effective in extracting information from real data.
- They can be generalized (but not without difficulty) to problems of higher dimensionality as long as a suitable forward model exists.
- They are stable with respect to noise.

### 3.3. Disadvantages

- They are not true inverse methods in the sense that only solutions to the forward problem are computed.
- They provide no statement about uniqueness.
- The minima which are found may be only local, not global, minima.
- They are time-consuming and tedious to implement.

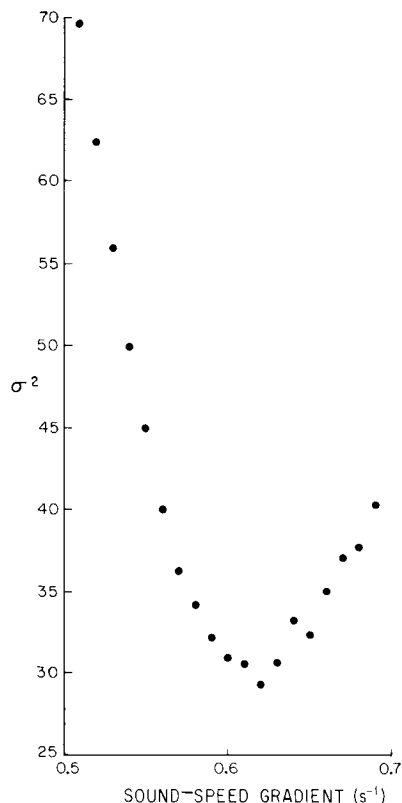


Fig. 8. Mean square difference as a function of sound-speed gradient.

#### 4. Perturbative inversion methods

In this approach, which is equivalent to linearized Born inversion, the variation in geoacoustic parameters about assumed background values for these parameters are related to the variation in some measured field quantity about the values of this quantity computed for the background parameters. In each of the cases of interest, a Fredholm integral equation arises that can be solved using linear inverse theory. This approach also provides a natural theoretical framework for the determination of resolution and variance estimates of the solution. Time-of-flight ocean acoustic tomography [6] is an example of this class of techniques. We will discuss in detail reflection coefficient inversion and normal mode eigenvalue inversion.

##### 4.1. Reflection coefficient inversion

This is the first approach we will discuss which requires as input data the plane-wave reflection coefficient of the bottom as a function of horizontal wavenumber at a fixed frequency. This requirement adds another layer of complication to the inverse problem, which is discussed in detail in Refs. [7] and [8], since the plane-wave response must be determined from the point source response. In a deep water context, such as that described in section 3.1., this step is executed by numerically computing the inverse Hankel transform of measurements of the magnitude and phase of  $p(r)$  to obtain an estimate of the depth-dependent Green's function

$$g(k_r) = \int_0^\infty p(r) J_0(k_r r) r dr. \quad (9)$$

The values of  $g(k_r)$  are then used to estimate the reflection coefficient  $R(k_r)$  using eq. (8). An essential element of this procedure is the spatial Nyquist criterion that the field measurements be made on a range grid  $\Delta r \leq \lambda/2$ , where  $\lambda$  is the acoustic wavelength in water. This requirement is directly related to the fact that the Hankel transform inversion is approximately equivalent to beamforming with a real or synthetic aperture horizontal array [9].

Assuming that we have obtained an estimate of  $R(k_r)$ , we now proceed with a perturbative scheme for inferring the compressional wave speed, compressional wave attenuation, and density of the bottom as a function of depth [10,11]. The exact and background models are shown in Figs. 9(a) and 9(b), respectively.

Although the theory can be developed for the case where the parameters in both regions II and III are the unknowns to be determined [10] and  $\rho(z) \neq \rho_b(z)$ , for simplicity we assume that the only unknowns are the parameters  $c(z)$  and  $\alpha(z)$  in region II [i.e.,  $\rho(z) = \rho_b(z)$ ].

We now express

$$k(z) = k_b(z) + \delta k(z) + i\alpha(z), \quad (10)$$

where  $k(z) = \omega/c(z)$  and  $k_b(z) = \omega/c_b(z)$ . The quantities  $\delta k(z)$  and  $i\alpha(z)$  are small real and imaginary perturbations around  $k_b(z)$  since  $c(z)$  is close to the background value  $c_b(z)$  and the attenuation  $\alpha(z)$  is small compared to  $k_b(z)$  for marine sediments at the frequencies of interest. We can then show that [10,11]

$$\begin{aligned} & \frac{i(k_0^2 - k_r^2)^{1/2}}{\rho_0} [R_b(k_r) - R(k_r)] \\ &= \int_0^h \frac{k_b(z)}{\rho_b(z)} [\delta k(z) + i\alpha(z)] p_b(z) p(z) dz, \end{aligned} \quad (11)$$

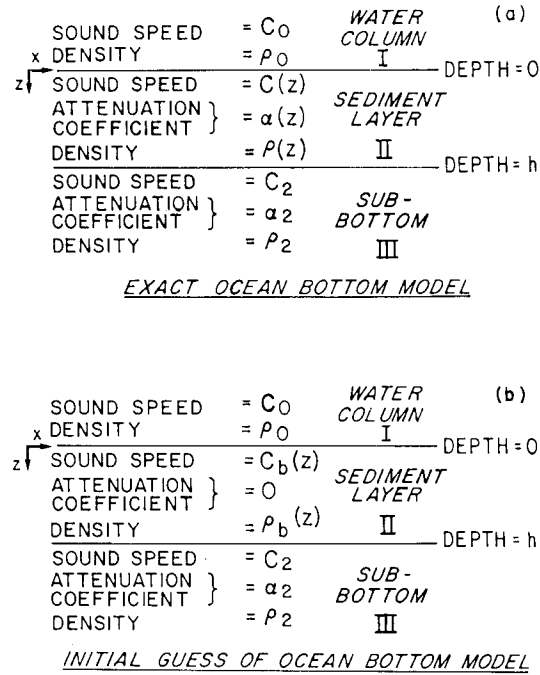


Fig. 9. The (a) exact and (b) background models for the bottom.

where  $R(k_r)$  and  $R_b(k_r)$  are the plane wave reflection coefficients for the exact and background models, respectively. Similarly,  $p(z)$  and  $p_b(z)$  are the exact and background pressure fields, respectively, in region II. Equation (11) is a nonlinear equation which we linearize by applying the Born approximation, i.e., we set  $p(z) = p_b(z)$ . It can be shown that the region of validity of this approximation corresponds to angles of incidence  $\theta$  ( $k_r = k_0 \sin \theta$ ) which are pre-critical with respect to the subbottom [10].

In the Born approximation, eq. (11) is in the form of a Fredholm integral equation of the first kind to which linear inverse theory can be applied. Specifically, given that the measured reflection coefficient is typically available only at a discrete set of horizontal wavenumbers [7]  $R(k_{r_n}), n = 1, \dots, N$ , we have

$$d_n = \int_0^h q(z)G_n(z) dz, \quad n = 1, \dots, N, \quad (12a)$$

where

$$d_n = \frac{i(k_0^2 - k_{r_n}^2)^{1/2}}{\rho_0} [R_b(k_{r_n}) - R(k_{r_n})], \quad (12b)$$

$$G_n(z) = \frac{k_b(z)}{\rho_b(z)} p_b^2(k_{r_n}, z), \quad (12c)$$

and

$$q(z) = \delta k(z) + i\alpha(z). \quad (12d)$$

Equation (12) is solved using a regularization method with a smoothness constraint [10,11]. We demonstrate the application of the method to the simultaneous reconstruction of sound speed and attenuation profiles. The quantities  $R(k_r)$ ,  $R_b(k_r)$ , and  $p_b(k_r, z)$  were computed at 25 Hz for 20 pre-critical angles using a propagator matrix method for the profiles shown in fig. 10. The background attenuation profile was assumed zero. The excellent agreement between the exact and reconstructed profiles is evident in fig. 10.

Additional examples which show the stability of the method with respect to the introduction of noise and computations of the resolution width can be found in Refs.[10] and [11].

#### 4.2. Normal mode eigenvalue inversion

When an experiment of the type described in section 3.1 is conducted in shallow water, the surface-reflected and water multiple arrivals cannot be gated out, and we observe the full steady-state field excited in the waveguide. Under these circumstances, the depth-dependent Green's function assumes a more complicated form which, for the case of an isovelocity water column with thickness  $h$  and a pressure-release surface at  $z = 0$ , is given by [12]

$$g(k_r) = \frac{e^{ik_z z_-} - e^{ik_z z_+} + R(k_r)e^{2ik_z h} [e^{-ik_z z_+} - e^{-ik_z z_-}]}{-ik_z [1 + R(k_r)e^{2ik_z h}]}, \quad (13)$$

where  $z_+ = z + z_0$ ,  $z_- = |z - z_0|$ , and we note that in this section  $z$  increases downward, so that  $z_0$  and  $z$  are source and receiver *depths* below the surface. Because there is now a nonlinear relationship between  $g(k_r)$  and  $R(k_r)$ , the problem of determining  $R(k_r)$  from measurements of  $p(r)$  is ill-posed [12,13], and instead of pursuing reflection coefficient inversion, we capitalize on a different, important feature of the Green's function. Specifically, the denominator of eq. (13) when set equal to zero is the well known characteristic equation governing the propagation of normal modes in an isovelocity water column overlying an arbitrary horizontally stratified bottom [12]:

$$1 + R(k_r)e^{2ik_z h} = 0. \quad (14)$$

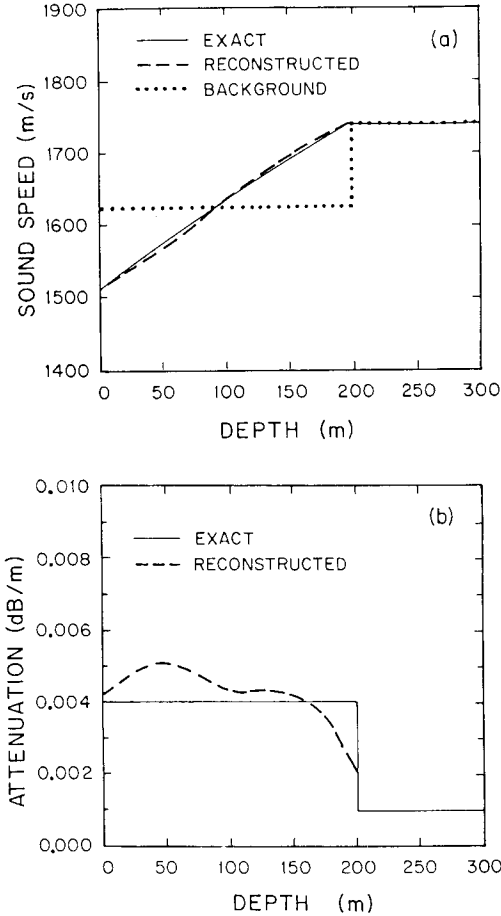


Fig. 10. Exact and reconstructed (a) sound speed and (b) attenuation profiles.

The Green's function will therefore have a discrete set of resonances occurring at the poles of  $g(k_r)$  which give rise to the discrete part of the spectrum in a normal mode representation of the field:

$$p(r) = i\pi \sum_n a_n \phi_n(z_0) \phi_n(z) H_0^{(1)}(k_n r). \quad (15)$$

The eigenfunctions  $\phi_n$  and eigenvalues  $k_n$  satisfy the equation

$$\left[ \frac{d^2}{dz^2} + k_0^2(z) - k_n^2 \right] \phi_n(z) = 0 \quad (16)$$

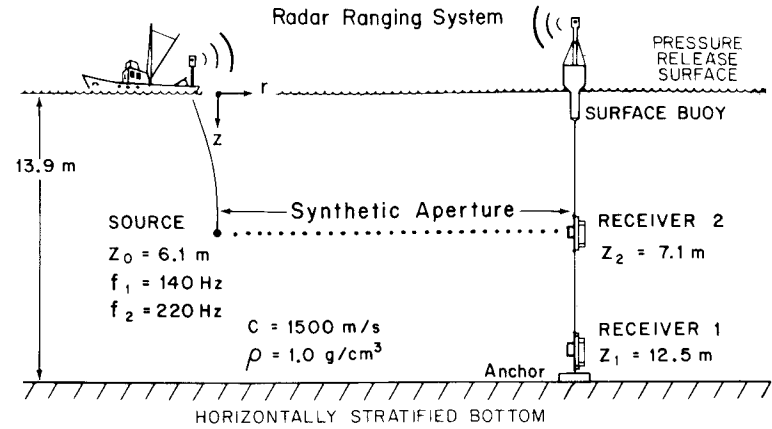


Fig. 11. Experimental configuration for the Nantucket Sound experiment.

along with impedance boundary conditions at the interfaces. Here  $H_0^{(1)}$  is the zero order Hankel function of the first kind,  $a_n$  is the modal normalization constant, and  $k_0(z)$  is the water wavenumber.

Since the modal eigenvalues are intimately related to the acoustic properties of the bottom, they can be used as the basis for a perturbative inversion scheme for determining the bottom parameters [10,14,15]. We will describe this technique only for compressional wave speed inversion, although it can be used for inferring compressional wave attenuation and density as well. Assuming a background model with  $k_b(z) = \omega/c_b(z)$  and density  $\rho_b(z)$  and an exact model with

$$k(z) = \frac{\omega}{c(z)} = \frac{\omega}{c_b(z) + \delta c(z)}, \quad (17)$$

we use first-order perturbation theory to obtain

$$k_n - k_{nb} = \frac{1}{k_{nb}} \int_0^\infty |\phi_{nb}(z)|^2 \frac{k_b^2(z)}{\rho_b(z)} \frac{\delta c(z)}{c_b(z)} dz, \quad (18)$$

where the  $k_n$  are the measured eigenvalues and  $k_{nb}$  and  $\phi_{nb}(z)$  are the eigenvalues and eigenfunctions computed for the background model. Again we have a Fredholm integral equation of the first kind to which linear inverse theory can be applied. This approach has been studied extensively and applied to both synthetic and experimental data [10,14,15]. For example, measurements were made in Nantucket Sound, Massachusetts at 140 and 220 Hz using the experimental configuration shown in fig. 11.

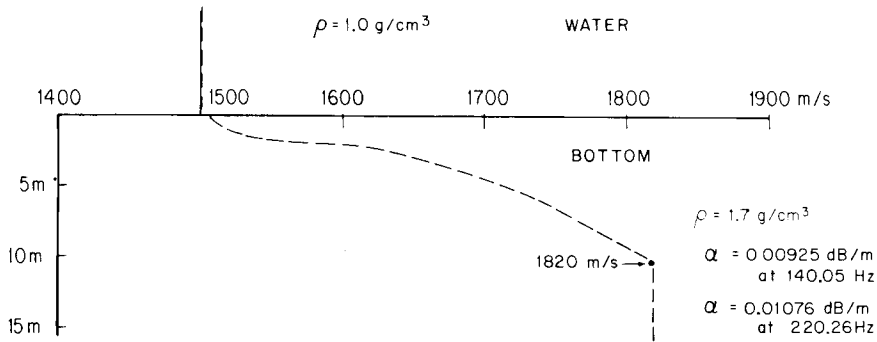


Fig. 12. Geoacoustic model inferred from the data using perturbative inversion.

The geoacoustic model inferred from the data using perturbative inversion with  $\rho_b = 1.7 \text{ g/cm}^3$  and  $c_b = 1820 \text{ m/s}$  is shown in fig. 12.

The corresponding comparisons between the theoretically computed and experimentally measured pressure field magnitudes and Green's functions at 140 Hz are shown in Figs.13 and 14, respectively.

Comparable, excellent agreement also occurs at 220 Hz. The variance associated with the sound speed estimate is shown in fig. 15.

Particularly noticeable is the sharp increase in the variance at about six meters depth into the sediment. This corresponds to the maximum turning depth for the modes used in the inversion. Below this depth, the wave fields are evanescent and therefore carry less information about the bottom properties.

#### 4.3. Advantages

- Perturbative inversion methods utilize most or all of the data available.
- They are straightforward to implement because of the existing machinery associated with linear inverse theory, which also provides resolution and variance estimates.
- They are effective in applications to real data.
- They can sometimes be generalized to problems of higher dimensionality.
- They are stable with respect to noise.

#### 4.4. Disadvantages

- Their effectiveness depends on the judicious choice of the background model parameters.
- They have limited uniqueness properties which are associated with the imposed constraints.

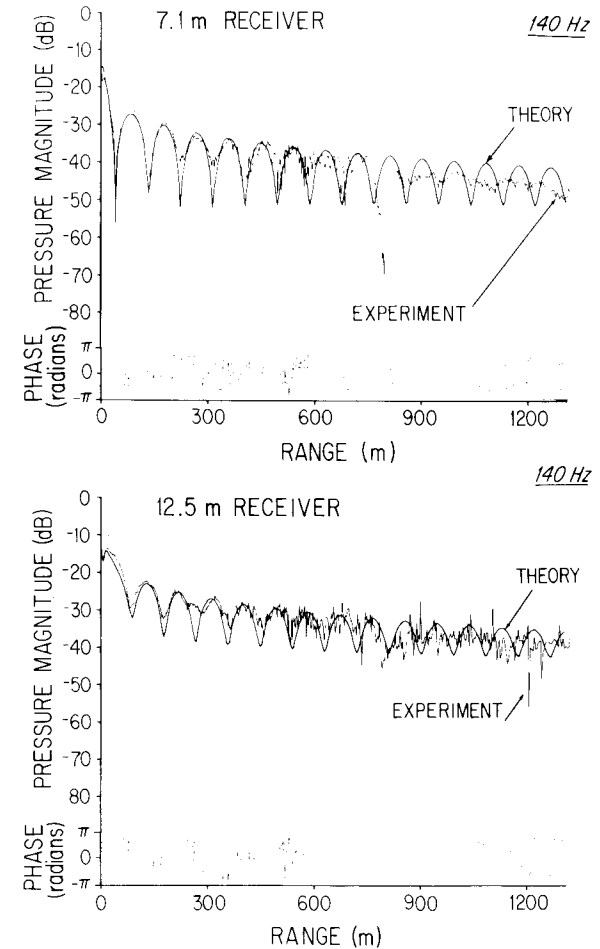


Fig. 13. Comparison of theoretical and experimental pressure fields.

## 5. Exact inverse methods

These methods are exact in the sense that they are non-perturbative and therefore require only weak, general assumptions about the nature of the unknown geoacoustic parameters. They also typically have associated with them uniqueness theorems which clearly describe the type of input data required to produce unique estimates of certain parameters. Examples of these techniques are the trace method [16] and the Gelfand-Levitan method [17,18], which we will now discuss in more detail.

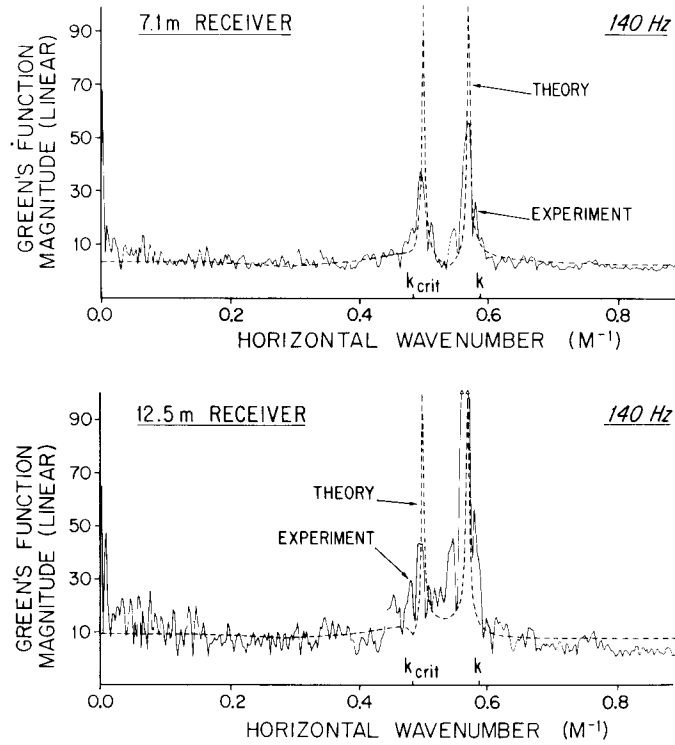


Fig. 14. Comparison of theoretical and experimental Green's functions.

### 5.1. Gelfand-Levitan method

The Gelfand-Levitan method was originally developed in a quantum mechanical context associated with determining the potential  $V(z)$  in the Schrödinger equation from scattering data [17]. Most applications to seismic inversion problems have required the impulse response of the bottom [i.e., the plane wave reflection coefficient  $R(\omega)$  as a function of frequency] at fixed angles of incidence as input data [19]. Under these circumstances, if  $R(\omega)$  is known for *all* frequencies at two pre-critical angles, the sound speed and density versus depth can be uniquely recovered. The principal obstacle to the successful application of this method to experimental data has been the bandwidth limitation associated with real seismic sources. Specifically, low-frequency energy, which yields important trend information in the inferred profiles, is lacking. Recently, there has been interest in the application of the Gelfand-Levitan method to narrowband input data for varying angles of incidence [18]. Then if  $R(k_z)$  is known for all  $k_z$  at

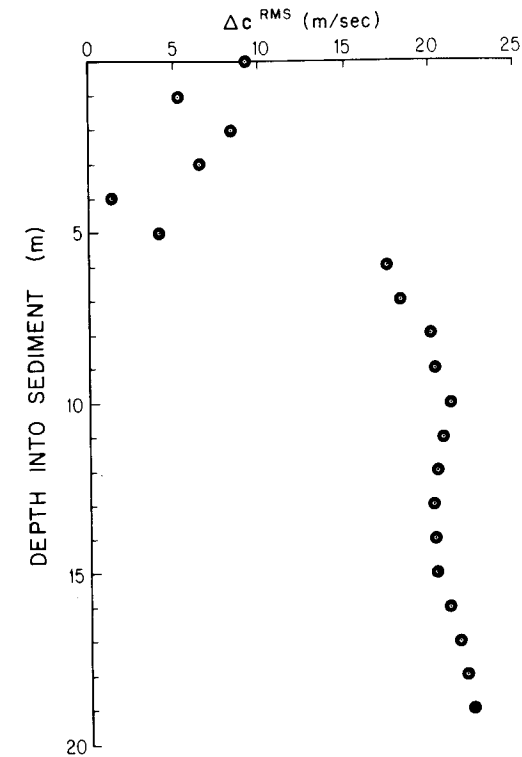


Fig. 15. Variance associated with the compressional wave speed estimate in fig. 12.

two frequencies, the sound speed and density profiles can be uniquely recovered. Reference [18] extensively explores the narrowband, oblique incidence problem both in terms of addressing the relevant theoretical considerations and in carrying out extensive studies on synthetic data. A principal finding of this work is that the narrowband case does not have the intrinsic bandwidth limitation of the broadband case. This is due to the fact that the relevant bandwidth in the narrowband case is in  $k_z$  (i.e., angle), not  $\omega$ . Then the trend information is obtained from post-critical, low  $k_z$  (analogous to low  $\omega$ ) data which, in principle, can be obtained using Hankel transform inversion of measured point source fields (cf. Sections 3.1. and 4.1.). To date, the implementation of the narrowband approach on real data has not been achieved because of the inability to perform a sufficiently well-controlled experiment for measuring the reflection coefficient in an ocean environment.

We shall review the steps in the oblique incidence inversion scheme, as-

suming a known constant density throughout the medium. The first step involves the computation of  $\tilde{R}(z)$ , which consists of two terms:

$$\tilde{R}(z) = \frac{1}{2\pi} \int_{-\infty}^{\infty} R(k_z) e^{-ik_z z} dk_z - i \sum_{n=1}^N r_n e^{-ik_{z,n} z}. \quad (19)$$

The first term is the Fourier transform of the reflection coefficient, which is usually computed using the FFT algorithm, while the second term is the sum of the residues for any perfectly trapped modes (bound states) excited in low velocity zones in the bottom. For typical cases of interest, the second term can be ignored. The second step requires the solution of the Gelfand-Levitan integral equation:

$$K(z, y) = -\tilde{R}(x+y) - \int_{-\infty}^z K(z, x) \tilde{R}(x+y) dx. \quad (20)$$

Equation (20) is a Fredholm integral equation of the second kind which, in general, is solved numerically, but can be solved approximately using the method of successive approximations. The latter procedure yields the following result for the potential:

$$V(z) = -2 \frac{d\tilde{R}(2z)}{dz} + 4\tilde{R}^2(2z) + \dots \quad (21)$$

The first term in eq. (21) is simply the Born approximation, since

$$-2 \frac{d\tilde{R}(2z)}{dz} = \frac{2i}{\pi} \int_{-\infty}^{\infty} k_z R(k_z) e^{-2ik_z z} dk_z. \quad (22)$$

The improved Born approximation in eq. (21) is useful computationally and also demonstrates the nonlinear nature of the inversion process. Finally, the sound speed in the bottom  $c(z)$  is calculated using the equations

$$V(z) = 2 \frac{dK(z, z)}{dz}, \quad (23a)$$

and

$$V(z) = k_0^2 [1 - n^2(z)], \quad (23b)$$

where  $n(z) = c_0/c(z)$ , and  $c_0$  is the sound speed in the water.

We demonstrate the application of the method for three examples at 25 Hz using synthetically generated reflection coefficients as input data.

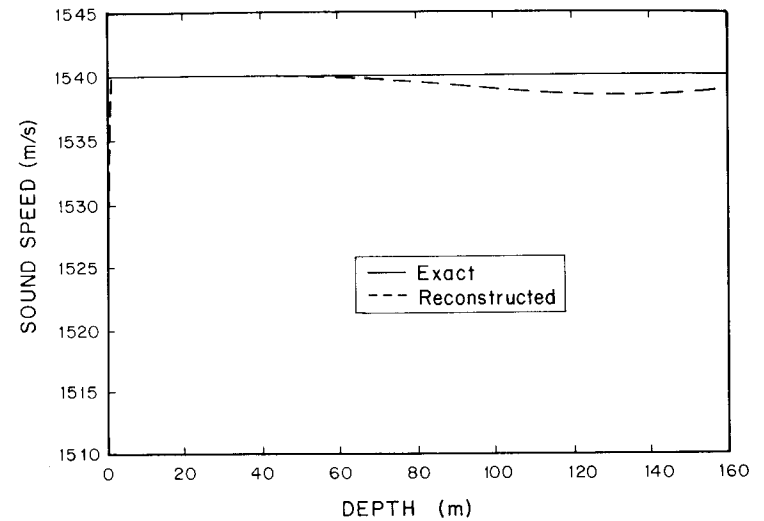


Fig. 16. Gelfand-Levitan reconstruction for an isovelocity half-space.

Figure 16 shows the excellent reconstruction for an isovelocity half-space, where  $c_0 = 1510$  m/s.

In fig. 17, the exact, continuous, linear-gradient profile was approximated by a sequence of homogeneous layers, each 6 m thick, so that  $R(k_z)$  could be computed using a propagator matrix method. Remarkably, the inverse technique reconstructed the stair-step structure, even though the incident wavelength was about 60 m ( $c_0 = 1540$  m/s). This is due to the fact that the *probing* wavelength is  $\lambda_z = \lambda \cos \theta$ , which ranges from zero at grazing incidence to  $\lambda$  at normal incidence.

In fig. 18, the stability of the algorithm with respect to noise, as well as the use of the improved Born approximation, are shown for a step potential. Here, zero-mean Gaussian noise with a standard deviation of 0.1 was added to the reflection coefficient in the lower figure.

## 5.2. Advantages

- Exact inverse methods utilize most or all of the data available.
- They are non-perturbative and therefore do not require a detailed background model.
- They provide uniqueness theorems which are typically stated for unrealizable conditions (e.g., infinite bandwidth), but are nevertheless useful as a guide in designing inversion schemes.

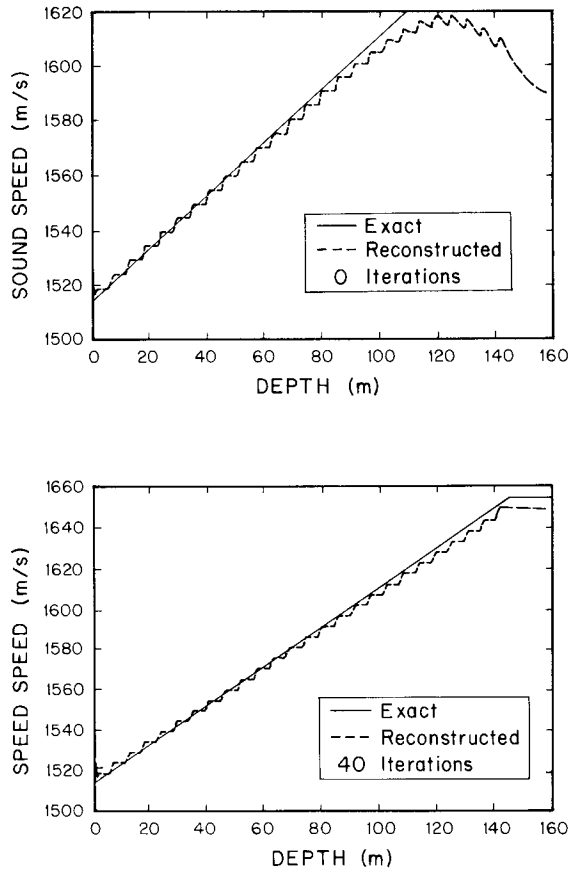


Fig. 17. Gelfand-Levitan reconstruction for a linear velocity gradient approximated by homogeneous layers.

### 5.3. Disadvantages

- They are difficult to implement on real data.
- They are difficult to generalize to problems of higher dimensionality.
- They are sometimes unstable with respect to noise (e.g., in the broadband case).

## 6. Conclusions

We have seen that a variety of inverse methods are used in ocean bottom acoustics, each of which has its advantages and disadvantages. Because

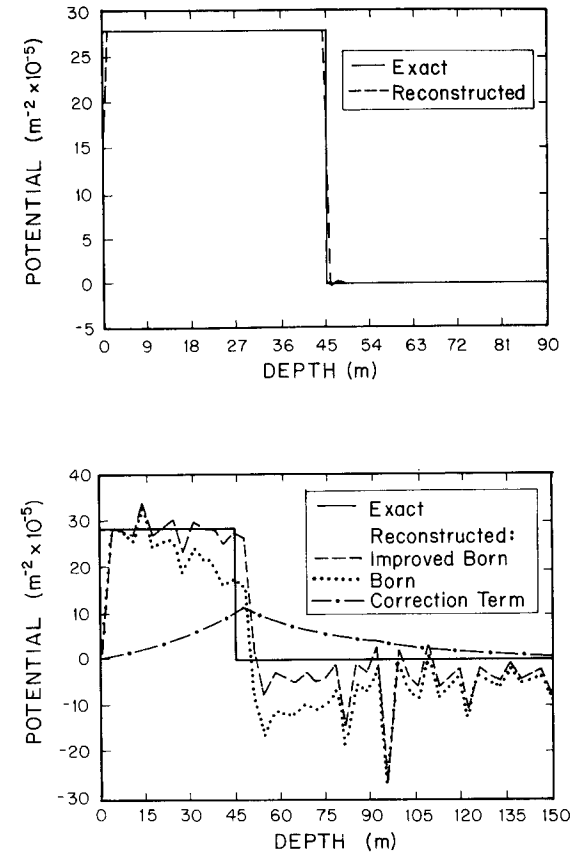


Fig. 18. Gelfand-Levitan reconstruction for a step potential with and without noise.

no single class of techniques is ideal, it is important to use as many measurement methods and suitable inversion schemes as possible in inferring a geoacoustic model. We must also recognize that although specific feature and iteration of forward model methods have been and will continue to be useful, we are entering a new era where the more powerful perturbative and exact methods will dominate our approach to solving inverse problems.

## References

- [1] K. Aki and P.G. Richards, *Quantitative Seismology Theory and Methods*

- (Freeman, San Francisco, 1980).
- [2] G.V. Frisk, "Determination of Sediment Sound Speed Profiles Using Causitic Range Information", in *Bottom-Interacting Ocean Acoustics*, edited by W.A. Kuperman and F.B. Jensen (Plenum, New York, 1980).
  - [3] G.V. Frisk, J.A. Doult, and E.E. Hays, "Bottom Interaction of Low-Frequency Acoustic Signals at Small Grazing Angles in the Deep Ocean", *J. Acoust. Soc. Am.* 69,(1981) 84-94.
  - [4] A.Tarantola, *Inverse Problem Theory* (Elsevier, Amsterdam, 1987).
  - [5] G.V. Frisk, J.A. Doult, and E.E. Hays, "Geoacoustic Models for the Icelandic Basin," *J. Acoust. Soc. Am.* 80, (1986) 591-600.
  - [6] W.Munk and C.Wunsch, "Ocean Acoustic Tomography: A Scheme for Large Scale Monitoring," *Deep-Sea Research* 26A, (1979) 439-464.
  - [7] G.V. Frisk, A.V. Oppenheim, and D.R. Martinez, "A Technique for Measuring the Plane-Wave Reflection Coefficient of the Ocean Bottom," *J. Acoust. Soc. Am.* 68, (1980) 602-612.
  - [8] D.R. Mook, "The Numerical Synthesis and Inversion of Acoustic Fields Using the Hankel Transform with Application to the Estimation of the Plane Wave Reflection Coefficient of the Ocean Bottom," Sc.D. Thesis, MIT/WHOI Joint Program, Cambridge, MA and Woods Hole, MA (January 1983).
  - [9] G.V. Frisk, J.F. Lynch, G.J. Tango, and M.F. Werby, "Mapping Seafloor Geoacoustic Properties in Shallow Water From Monochromatic Pressure Field Data: Two Methods Based on Hankel Transform Inversion," *Proceedings of 18th Annual Offshore Technology Conference*, 445-452 (1986).
  - [10] S.D. Rajan, "An Inverse Method for Obtaining the Attenuation Profile and Small Variations in the Sound Speed and Density Profiles of the Ocean Bottom," Ph.D. Thesis, MIT/WHOI Joint Program, Cambridge, MA and Woods Hole, MA (May 1985).
  - [11] S.D. Rajan and G.V. Frisk, "An Inverse Method for Obtaining the Attenuation Profile and Small Variations in the Sound Speed and Density Profiles of the Ocean Bottom," in *Progress in Underwater Acoustics*, edited by H.M. Merklinger (Plenum, New York, 1987).
  - [12] G.V. Frisk and J.F. Lynch, "Shallow Water Waveguide Characterization Using the Hankel Transform," *J. Acoust. Soc. Am.* 76, (1984) 205-211.
  - [13] M.S. Wengrovitz, "The Hilbert-Hankel Transform and Its Application to Shallow Water Ocean Acoustics," Sc.D. Thesis, MIT/WHOI Joint Program, Cambridge, MA and Woods Hole, MA (January 1986).
  - [14] S.D. Rajan, J.F. Lynch, and G.V. Frisk, "Perturbative Inversion Methods for Obtaining Bottom Geoacoustic Parameters in Shallow Water," *J. Acoust. Soc. Am.* 82, (1987) 998-1017.
  - [15] J.F. Lynch, S.D. Rajan, and G.V. Frisk, "A Perturbative Inverse Method

- for the Determination of Geoacoustic Parameters in Shallow Water," in *Progress in Underwater Acoustics*, edited by H.M. Merklinger (Plenum, New York, 1987).
- [16] D.C. Stickler, "Inverse Scattering in a Stratified Medium," *J. Acoust. Soc. Am.* 74, (1983) 994-1005.
  - [17] I.M. Gelfand and B.M. Levitan, "On the Determination of a Differential Equation from its Spectral Function," *Izv. Akad. Nauk SSSR* 15, (1951) 309-360; *Am. Math. Soc. Transl.* 1, (1955) 253-304.
  - [18] A. A. Merab, "Exact Reconstruction of Ocean Bottom Velocity Profiles from Monochromatic Scattering Data," Sc.D. Thesis, MIT/WHOI Joint Program, Cambridge, MA, and Woods Hole, MA (January 1987).
  - [19] J.A. Ware and K. Aki, "Continuous and Discrete Inverse Scattering Problems in a Stratified Elastic Medium," *J. Acoust. Soc. Am.* 45, (1969) 911-921.